Investigation of the Angular Correlation in the $C^{12}(p,2p)B^{11}$ Reaction at 45.5 MeV*

KENNETH E. RICHIE† AND BYRON T. WRIGHT
Physics Department, University of California, Los Angeles, California
(Received 6 February 1967)

The angular-correlation and energy distributions of the protons emitted from the $C^{12}(p,2p)B^{11}$ reaction at 45.5 MeV were measured with an absolute uncertainty of 10% and an angular resolution of $\pm 2.5°$. The data are compared with computer calculations based on a parameter study of the distorted-wave t-matrix approximation theory. Excellent agreement is obtained provided either the optical-model potential or the nuclear size is overestimated.

I. INTRODUCTION

IT has been recognized for some time that the direct interaction is the primary mechanism involved in proton-induced reactions at intermediate energies,[1] i.e., the incoming proton interacts with only a few of the nucleons in the initial nucleus, the reaction going directly to the final state without formation of an intermediate state. However, accurate predictions of reaction yields have been difficult in this energy region. This report attempts to study the suitability of the distorted-wave approximation in describing the reaction. The energy and angular correlations in the $C^{12}(p,2p)B^{11}$ reaction were measured and compared with the theoretical predictions. The $(p,2p)$ reaction in particular is favorable to a direct interaction since if a compound nucleus were to be formed, the reaction would be suppressed by the Coulomb barrier.

In the direct interaction picture the $(p,2p)$ reaction can be considered as a p-p collision modified by certain nuclear effects. The latter can be subdivided roughly into three groups: Nuclear structure, since one proton is bound in the initial nucleus; proton-nuclear core interactions in the initial and final states; and the possible modification of the two-body force by the presence of other nucleons.

The analysis of the angular correlation of the two emitted protons is simplest at high-incident energies, since the reaction most closely resembles free p-p scattering there. Adequate analyses for this case have been made by using classical kinematic calculations,[2] modified to the extent that the bound proton is represented by a reasonable momentum distribution function. A parallel quantum-mechanical treatment can be made using a plane-wave Born approximation. The wave functions for the free protons are treated as plane waves, with the appropriate momenta, and the bound-proton wave function is calculated from a potential well representing the interaction of the bound proton with the rest of the nucleus. The matrix element for the $(p,2p)$ transition is then:

$$M_L{}^m = \int d\mathbf{r}_1 d\mathbf{r}_2 [\exp(i\mathbf{k}_1\cdot\mathbf{r}_1)\exp(i\mathbf{k}_2\cdot\mathbf{r}_2)]^* V(\mathbf{r}_1-\mathbf{r}_2) \times \exp(i\mathbf{k}_0\cdot\mathbf{r}_1)\psi_L{}^m(\mathbf{r}_2)\int d\tau\, \phi_{A'}{}^*(\tau)\phi_{A'}(\tau), \quad (1)$$

where $\mathbf{k}_0$, $\mathbf{k}_1$, $\mathbf{k}_2$ are the initial and final proton momenta, respectively, and $\psi_L{}^m(\mathbf{r}_2)\phi_{A'}{}^*(\tau)$ is the wave function of the initial nucleus separated into the bound-proton wave function and the residual nucleus wave function.

Assuming the struck proton to have an initial momentum $\mathbf{q}=\mathbf{k}_0-\mathbf{k}_1-\mathbf{k}_2$, then the matrix element reduces to

$$M_L{}^m = \int d\mathbf{r}\exp(-i\mathbf{k}_1\cdot\mathbf{r})V(\mathbf{r})\exp(+i\mathbf{k}_0\cdot\mathbf{r}) \times \int d\mathbf{r}'\exp(-i\mathbf{q}\cdot\mathbf{r}')\psi_L{}^m(\mathbf{r}'), \quad (2)$$

where $\mathbf{r}=\mathbf{r}_1-\mathbf{r}_2$ and $\mathbf{r}'=\mathbf{r}_2$.

The $(p,2p)$ cross section is then

$$d\sigma_{p,2p} = d\sigma_{p,p}(\mathbf{k}_0,\mathbf{q};\mathbf{k}_1,\mathbf{k}_2)P_L{}^m(\mathbf{q}), \quad (3)$$

i.e., the cross section for p-p scattering from state $\mathbf{k}_0$ to state $\mathbf{k}_1$ by a bound proton of momentum $\mathbf{q}$ multiplied by the probability of finding a bound proton with momentum $\mathbf{q}$.

The angular-dependence results primarily from variation of the second term. The use of reasonable potentials, e.g., a harmonic-oscillator well, leads to the gross features of the $(p,2p)$ angular correlation.

At intermediate energies the quasifree scattering approximation is no longer valid and the interaction must include the nuclear effects mentioned earlier. The distorted-wave approximation takes the proton-nuclear core interactions into account by assuming the protons are subject to optical-model potentials in the initial and final states. The free-proton wave functions are then distorted rather than plane waves. Lim and McCarthy[3] have calculated the angular correlation in the distorted-wave-impulse approximation which uses an effective

* Supported in part by the U. S. Office of Naval Research, under Contract No. Nonr-233(44).

† Present address: Physics Department, University of California, Santa Barbara.

[1] R. M. Eisberg and G. Igo, Phys. Rev. **93**, 1039 (1954).

[2] O. Chamberlain and E. Segrè, Phys. Rev. **87**, 81 (1952).

[3] K. L. Lim and I. E. McCarthy, Phys. Rev. Letters **13**, 446 (1964).

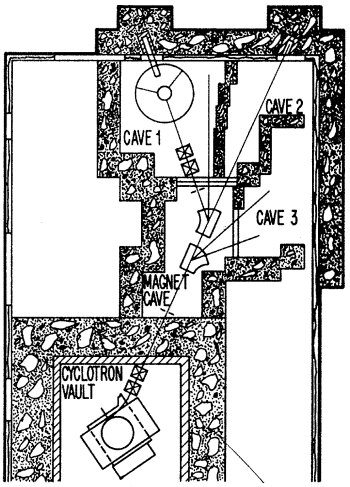

FIG. 1. University of California at Los Angeles cyclotron laboratory south experimental area.

potential derived from the t matrix for p-p scattering. They also have developed a computer program to obtain numerical results. The matrix element in the single-particle model is

$$M_L{}^m = \int d\mathbf{r}_2 d\mathbf{r}_1 \chi_0(\mathbf{r}_1,\mathbf{k}_0)\chi_L{}^*(\mathbf{r}_1,\mathbf{k}_L)\chi_R{}^*(\mathbf{r}_2,\mathbf{k}_R) \times t(\mathbf{r}_1-\mathbf{r}_2)\psi_L{}^m(\mathbf{r}_2), \quad (4)$$

where χ_0, χ_L, and χ_R are the optical-model wave functions for the incident, left, and right protons respectively, and $t(r)$ is the effective two-body force. The two-body force is represented by a pseudopotential consisting of three Yukawa potentials which correspond to one-, two-, and four-pion exchange:

$$t(r) = -83\left[\frac{\exp(-0.73r)}{0.73r} - 5.0\frac{\exp(-1.5r)}{1.5r} + 20\frac{\exp(-3.0r)}{3.0r}\right]. \quad (5)$$

The pseudopotential parameters were determined by fitting p-p scattering at 90° at energies up to 300 MeV.

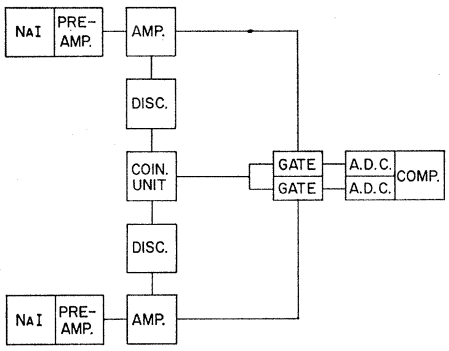

FIG. 2. Block diagram of electronics.

The $C^{12}(p,2p)B^{11}$ reaction at 45 MeV should be an excellent means for investigating the distorted-wave theory. The energies of the two emitted protons can be determined with sufficient accuracy to determine the final state. In addition the incident energy is low enough for the nuclear effects to be appreciable, and yet high enough to assure a direct interaction.

The purpose of the experiment then was to produce a set of angular correlation data selected to best meet the conditions prescribed by the theory, as discussed in the next section. The results of the experiment are presented in Sec. III. Section IV describes the comparison of the theory with the data and examines the information obtained.

II. EXPERIMENTAL PROCEDURE

The negative-ion facility of the UCLA cyclotron laboratory was used to obtain appropriate proton beams for a low-yield reaction study. The operation of the negative ion mode has been described.[4]

The negative hydrogen ions are accelerated and passed through a 0.0005-in. beryllium foil which strips off the two electrons, allowing the remaining proton to be bent out of the cyclotron by the magnetic field. Fig. 1 shows the cyclotron and the negative-ion experimental area.

After a small amount of energy analysis by the cyclotron magnetic fringe field the beam passes through a 0.0005-in. (H) [Dupont Kapton Polymide Film, Dupont Co., Circleville, Ohio] foil into a 4-in. beam pipe. A quadrupole doublet focuses the beam to a waist at a set of adjustable copper slits outside of the cyclotron vault. These slits are typically 0.3×0.3 in. and transmit approximately 10% of the beam into the two bending magnets. The second-bending magnet is used to deflect the beam through 45 deg, energy analyze the beam and focus it to a second pair of slits 13 ft in front of the target. The beam passes out of the magnet cave through a hole in 6.5 in. of armor plate into a second quadrupole doublet which focuses the beam to an image about $\frac{3}{16}$ in. wide and $\frac{3}{8}$ in. high at the center of the scattering chamber.

After passing through the scattering chamber the beam is stopped in a Faraday cup 8 ft from the target. The entrance to the cup is a 0.002-in. H foil window five inches in diameter. A 5-in.-long and 4.5-in.-diam aluminum cylinder is placed in front of the collector and kept at −1000 V to prevent secondary electron emission. The cup is maintained at approximately 10^{-5} mm of mercury pressure to prevent residual gas ionization. Two half disks, each intercepting about one-third of the current, are placed in the back of the Faraday cup to monitor the left-right symmetry of the beam. The beam current is integrated on an Elcor model A 309A current indicator and integrator.

[4] A. C. Paul and B. T. Wright, IEEE Trans. Nucl. Sci., NS-13 74 (1966).

The shielding of the magnet cave, absence of defining slits near the scattering chamber, and the Faraday cup geometry combine to establish a very low background level.

The scattering stand consists of a cylindrical center post bolted perpendicular to the floor, and an 8 ft.-diam. circular track on which are two arms. The arms are supported on the track by remotely controlled motor driven wheels. Backlash effects are removed by always moving the arms toward larger angles when going to the desired positions. The reproduction of the angular readout was better than 0.1 deg. The zero angle or beam direction was measured by comparing elastic-scattering cross sections on the two sides of the beam.

The beam energy was measured by the cross-over technique.[5] The scattering angles for which the inelastic 4.4 and 9.6-MeV peaks from carbon correspond to elastic proton-proton scattering on hydrogen are observed on each side of the beam. The kinematics are then solved to find the initial energy. This value can be used to calibrate the bending magnets in terms of nuclear magnetic resonance measurements of the magnetic fields. In this experiment the energy was measured to be 45.5 MeV. The energy spread was about 200 keV (full width at half-maximum, FWHM).

The scattering chamber is a 10.75-in.-diam, 6-in.-high aluminum cylinder open at the top. A $\frac{3}{4}$-in. window extends from plus 165 deg to minus 165 deg and is enlarged to a circular opening of 1.5 in. diameter in the forward direction in order to prevent obstruction of the emerging beam. H-foil 0.002-in. thick was used to cover the windows since its properties best withstood radiation damage as well as hole development from flexing.

Adjustable slits with current readouts or glass plate holders for beam picture-taking, can be centered inside the chamber in order to align the beam. These and the two sets of preliminary slits were used before each run to determine the beam quality and alignment.

The chamber lid contains a target ladder holder, and a drive system for the vertical positioning of the holder and for rotating the system about a vertical line. Three targets are mounted in each target ladder. The target ladder is then fixed to the target holder in the chamber lid. The target zero angle is calibrated by measuring the elastic-scattering counting rate, which is proportional to the target thickness, versus the rotational position and observing the minimum. The drives and readouts for the target mechanism are remotely controlled and indicated.

The detectors were mounted on carriages which could be moved radially on each arm. The tangential variation of the radial movements were found to be less than 0.1 deg by theodolite observations. The detector was placed inside a lead cylinder of inside diameter two inches and outside diameter seven inches. The detector mounts are accurately pinned to the arms with shoulder bolts.

[5] B. M. Bardin and M. E. Rickey, Rev. Sci. Instr. **35**, 902 (1964); R. Smythe, Rev. Sci. Instr. **35**, 1197 (1964).

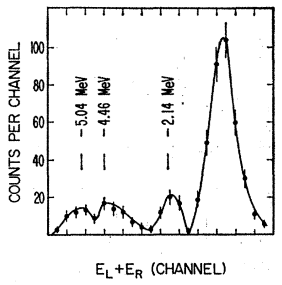

FIG. 3. Sum energy spectrum of the two emitted protons in the $C^{12}(p,2p)B^{11}$ reaction. The four peaks correspond to the ground state and the first three excited states of the residual nucleus.

Two NaI(Tl) crystals two inches in diameter and 0.5 in. thick were used. The crystals were commercially mounted by quartz pipes on RCA 8053 photomultiplier tubes surrounded by mumetal shields. The high-voltage input to the tubes and the signal output were made at the tube base. The output pulses were amplified by a preamplifier located only a few inches from the tube base. These signals were then carried by coaxial cable to an RIDL model 30–23 amplifier in the counting room.

The block diagram of the electronics is shown in Fig. 2. After amplification the output is split into linear and logic signals. The logic signal passes through a discriminator and into a coincidence unit which gives a positive 10-V output signal for pulses occurring within a variable time period. The output signal then opens each of two linear gates which allow the delayed linear signals from the amplifier pair to pass into the analog to digital-converter inputs of an on-line computer system. The pulse heights of the two signals are recorded and stored. In this manner the two major criteria for determining a $(p,2p)$ event are satisfied, i.e., the protons are emitted in coincidence and their energies are restricted by the kinematics of the problem:

$$E_L+E_R=E_0-E_B, \tag{6}$$

where E_L, E_R, and E_0 are the energies of the final left, final right, and initial protons; and E_B the energy required to release the bound proton.

The latter requirement brings out a very important feature of the $(p,2p)$ reaction at low-incidence energies. At higher energies, examination of the sum-energy spectra of the two protons shows broad peaks at binding energies of 16 and 36 MeV corresponding to ejection from the P and S shells of carbon.[6] However, the resolution was insufficient to determine whether or not the residual nucleus B^{11} was left in the ground state. The results of the improved energy resolution available at 45 MeV are shown in Fig. 3 where peaks corresponding to the B^{11} nucleus being left in the ground state and the first three excited states at 2.14, 4.46, and 5.04 MeV, respectively, are observed.

The resolution indicated allows the choice of events corresponding to unique transitions of a bound proton being ejected from the outer or P shell of C^{12} to a free proton and a B^{11} nucleus in a defined energy state.

[6] J. P. Garron, J. C. Jacmart, M. Riou, C. Ruhla, J. Teillac, and K. Strauch, Nucl. Phys. **37**, 126 (1962); and Phys. Rev. Letters **7**, 261 (1961).

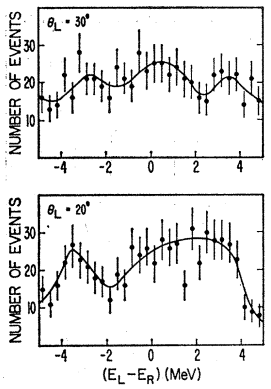

FIG. 4. Difference energy spectra of the two emitted protons in the $C^{12}(p,2p)B^{11}$ reaction. All events are taken from the ground-state peak in the sum energy spectrum (Fig. 3). $\theta_R=30°$.

Since the theory calculates ground-state to ground-state transitions only, we were able to compare it directly with experiment by selecting only those events.

The angular correlation of the protons differs for different final states because of the variation in angular and linear momentum transfer. Therefore a unique transition must be measured if a direct comparison with theory is to be attempted.

The optimum true to accidental ratio is obtained by relatively increasing the solid angles and decreasing the incident current and/or the target thickness. The angular apertures in the scattering plane were, however, restricted to 5°, resulting in an expected angular resolution of 5° FWHM which was confirmed by proton-proton scattering from hydrogen. The collimators were designed to optimize the ratio of solid angle to angular aperture by using a vertical dimension of $\frac{3}{4}$ in., and a horizontal dimension of $\frac{1}{2}$ in.

The target used was a 0.00125-in. CH foil. The use of thin targets not only reduced the accidental coincidence rate but also improved the energy resolution. Since the reaction can take place in either the front or the back of the target, the two protons can have an energy spread of the order of the amount of energy lost in traversing the target. In the case of two 15-MeV protons emitted at 30° with respect to the incident beam direction, the total energy loss is 280 keV for the target used.

Accidental coincidence rates were determined by inserting a 35.5-nsec delay in one channel of the coincidence unit. This delay equals the separation of adjacent beam bursts. The background rate was found to be essentially independent of the resolution of the coincidence unit up to a resolving time of 35 nsec. Because of this and in order to provide a safety margin for time jitter, the resolving time was adjusted to be between 30 and 35 nsec for all runs. The data runs were taken at a beam current of approximately one nA. At this current the accidental coincidence rate was negligible.

Since the cross section involves the number of events within a given energy interval for each proton, it was necessary to record the energies of each proton and also to do it over a large number of channels in order to reduce the error due to end-channel cutoff.

A computer program with the following features was developed to accumulate, store and treat the data: (a) A calibration mode, which allows each analog to digital converter on the computer to be calibrated individually on a 512-channel full scale, by signals of known energy (protons elastically scattered by hydrogen at different angles). The print out of this mode could be started and stopped at arbitrary preset channel numbers thus eliminating long print outs of unnecessary energy regions. (b) A prompt print-out mode in which each member of the pair of pulses is analyzed in a 1024-channel full scale and then immediately printed out with channel numbers in the following format: $x+y$, x, y, and $x-y$. (c) An ordering mode which orders all the coincident pairs at the end of a run in the same format as b, except that the largest sum is written first and the smallest difference is ordered first for cases where the sums are equal. In addition all equal sums are grouped and their number is recorded. Also recorded is the total number of events analyzed. The largest and smallest sums to be printed out as well as the largest difference can be preset.

The number of events versus the sum energy, for a preset maximum energy difference, was on live display on an oscilloscope (256 channels full scale). The data can be stored on tape. The calibration mode is also used for storage of elastic-scattering data obtained from carbon and hydrogen for normalization purposes.

The energy sharing of the two protons is important since it determines the final-state optical-model potentials which must be used in the analysis. Since the computer program of Lim and McCarthy used one potential in the final state, i.e., each proton is assumed to have the same energy, it was necessary to compromise between statistical errors and nonsymmetric energy sharing by selecting only those events for which the absolute energy difference of the two protons was 4 MeV or less.

III. RESULTS

The energy scale was calibrated by p-p scattering from hydrogen at several angles corresponding to the

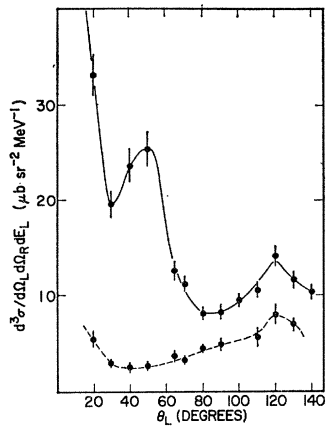

FIG. 5. The angular correlation of the two emitted protons in the $C^{12}(p,2p)B^{11}$ reaction. The full line connects points for g.s.-to-g.s. transitions with $|E_L-E_R|\leq 4$ MeV. The dashed line indicates the differential cross sections for transitions to the first-excited state of B^{11} with $|E_L-E_R|\leq 6$ MeV.

energy region of interest. The slope intercepts of the two analog-to-digital converters (ADC) were carefully adjusted with a pulser to give exactly the same channel number for a given pulse height. Small collimators were used in the calibration runs to avoid the kinematic energy spread associated with large angular openings.

Proton-proton coincidences from hydrogen were used to check the coincidence unit efficiency. The target thickness and beam intensity were monitored by elastic scattering from C^{12} using the cross sections measured at this laboratory.[7]

Holding the right detector fixed at 30°, the left detector was rotated from 20° to 140° on the other side of the beam in steps of about 10°. At each angle, the ground-state to ground-state events were chosen from the sum-energy spectrum (Fig. 3) and these were then plotted in terms of difference energy spectra (Fig. 4). There was an absence of sharp structure in the difference energy spectra, but the energy sharing versus angle did agree with direct-interaction theory, i.e., the left energy of the median event moved slowly toward lower energies as the left angle was increased.

The ground-state-to-ground-state differential cross sections for $|E_L-E_R|\leq 4$ MeV are shown in Fig. 5 (full line). The cross section for transitions into the first-excited state of B^{11} where $|E_L-E_R|\leq 6$ MeV are also shown (dashed line). The different correlations confirm the need for energy-level separation as discussed previously. Higher excited levels could not be accurately resolved.

All the statistical errors were between 7 and 8%. The absolute uncertainty was plus or minus 10%. The cross section was measured two or more times at each angle to further reduce any uncertainties in the data. The results for the different runs were found to be in good agreement. The differential cross section for g.s.-to-g.s. transitions were also calculated for asymmetric energy sharing of 2 and 6 MeV. The measurements at each angle were generally in good statistical agreement in all three cases.

Comparison to the 50-MeV symmetric geometry experiment performed at Berkeley[8] could be made in the case where both detectors were at 30°. The two experimental measurements were within statistical agreement. The over-all cross sections were of the same magnitude indicating small changes in cross section over a 5-MeV energy difference.

IV. DISTORTED-WAVE THEORY PARAMETER STUDY

An analysis of the reaction in terms of the distorted-wave theory has been made. The theoretical predictions of the angular correlation for various values of input parameters are compared with the experimental data. The calculations were made at the UCLA computer facility using a computer program supplied by McCarthy.[3]

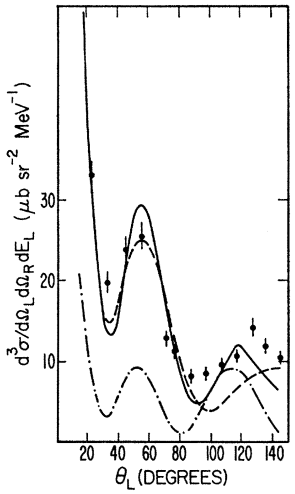

FIG. 6. Comparison of angular correlation curves calculated from set R (full line), set M (dashed line), and set E (dotted line), with the experimental data.

The important parameters to be considered were the final-state optical-model parameters (the radius, $R=R_fA^{1/3}$; the real well depth, V_f; and the imaginary well depth, W_f); the radius of the bound-state potential well, R_B; and the relative contributions and ranges of the three Yukawa terms in the pseudopotential. The initial-state optical-model parameters were very insensitive due to the small amount of distortion at the higher energy and its effect on only one proton. The depth of the bound-state potential well was related to its range to keep $V_BR_B^2$ constant. The computer calculated the rms radius of the bound-state wave function $\langle r\rangle$ from the finite square-well potential parameters. $\langle r\rangle$ varies approximately linearly with R_B.

Good fits to the experimental data could be obtained, but only through the use of optical-model parameters considerably different from those inferred from elastic-scattering experiments. The required overestimation of distortion effects were similar to those deduced in analyses by McCarthy.[9] All computations involve the sum of the triplet and singlet contributions using the triplet-to-singlet ratio $(A_{11}/A_{10})^2=\frac{1}{3}$ as in Ref. 9. The triplet contributions were generally at least an order of magnitude smaller than the singlet calculations, and in most cases a change to $(A_{11}/A_{10})^2=1$ has an insignificant change in the final sum.

Table I compares three sets of final-state optical-model parameters adjusted to an initial energy of 45.5

TABLE I. Final-state optical-model parameters.

	Set E	Set M	Set R
V_f (MeV)	58.0	73.5	65.0
W_f (MeV)	7.5	4.5	4.0
R (F)	1.2	1.2	1.2
b (F)	0.5	0.5	0.5

[7] H. Wilmes, University of California at Los Angeles Technical Report No. P–71, 1965 (unpublished).

[8] H. G. Pugh, D. L. Hendrie, M. Chabre, and E. Boschitz, Phys. Rev. Letters 14, 434 (1965).

[9] K. L. Lim and I. E. McCarthy, Nucl. Phys. 88, 433 (1966).

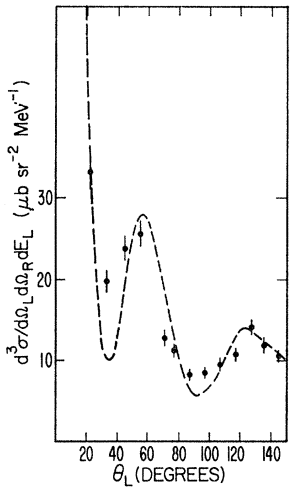

FIG. 7. The angular correlation calculated with V_F changed to 69.0 MeV from 73.5 MeV. (The curve is multiplied by a factor of 1.7.)

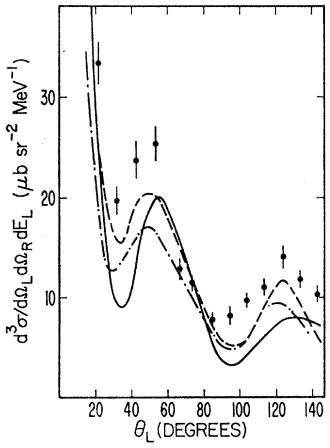

FIG. 8. The VR^2 ambiguities of the final-state optical-model potential. $V_F=71$ MeV, $R_F=1.2$ F (full line); $V_F=62$ MeV, $R_F=1.3$ F (dashed line); and $V_F=58$ MeV, $R_F=1.33$ F (dotted line).

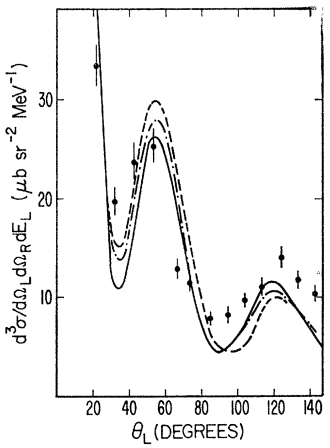

FIG. 9. The ambiguities between the real part of the final-state optical-model potential and the radius of the bound-state potential well. $V_F=65$ MeV, $\langle r\rangle=3.22$ F (full line); $V_F=69$ MeV, $\langle r\rangle=3.03$ F (dashed line); and $V_F=67$ MeV, $\langle r\rangle=3.09$ F (dotted line).

MeV, which best fit: elastic scattering (set E), the 50-MeV symmetric geometry experiment (set M), and the present experiment (set R).

Figure 6 compares the curves calculated from set R (full line), M (dashed line), and E (dotted line), with the experimental data. The major discrepancies in set R are the low magnitudes in the two minima and the second maximum. The increase in distortion, by increasing the potentials, has a progressively larger effect as the angle is reduced.

The second maximum could be obtained from set M by lowering the real part of the potential from 73.5–69.0 MeV. An excellent shape fit is obtained in this manner but the magnitude of the curve is lowered as the real potential is reduced. Figure 7 shows the predicted curve multiplied by a factor of 1.7.

In order to get the proper magnitudes either the real part of the potential or the radial extent had to be increased. The two parameters could be changed in an approximately VR^2 relationship without appreciably changing the relative features of the curve. Figure 8 shows the three curves for $V_f=71$ MeV, $R_f=1.2$ F (full line), $V_f=62$ MeV, $R_f=1.3$ F (dashed line), and $V_f=58$ MeV, $R_f=1.33$ F (dotted line). If R_f is held fixed at 1.2 F, a similar ambiguity occurs between V_f and the radius of the bound-state potential well. For example in set R the rms bound-state wave function radius was increased to 3.22 F from the value 2.79 obtained by McCarthy[3] in an analysis of higher-energy experiments. Figure 9 compares set R (full line) with the curves calculated for $V_f=69$ MeV, $\langle r\rangle=3.03$ F (dashed line), and $V_f=67$ MeV, $\langle r\rangle=3.09$ F (dotted line). The depth of the potential well was changed to keep $V_B R_B^2$ constant.

Continuing the VR^2 ambiguity in the optical-model parameters toward the elastic-scattering potentials, shape changes begin to occur when R_f becomes larger than 1.33 fm without any appreciable magnitude increase. Figure 10 shows the computed values for $R_f=1.33$ (solid line) and 1.4 F (dashed line), using the standard potential values $V_f=58$ MeV, $W_f=7.5$ MeV, and $\langle r\rangle=2.79$ F.

However, it was possible to obtain a good fit with the standard potential magnitudes by increasing the bound-state well radius again. In Fig. 11 the solid line is calculated from the standard potential magnitudes, $R_f=1.33$ F and $\langle r\rangle=3.10$ F. The dashed line shows the effect of reducing $\langle r\rangle$ to 3.04, and the dotted line corresponds to a change in $\langle r\rangle$ to 3.23 F.

Using the parameters for the best fit in Fig. 11, any changes in the relative magnitudes and/or ranges of the three terms in the pseudopotential resulted in considerably poorer fits to the data both in shape and magnitude. Equally poor fits were obtained by adjusting the pseudopotential parameters while using the standard set (E) for the optical model and $\langle r\rangle=2.79$ F.

The next attempts were directed toward finding possible fits using the standard optical-model param-

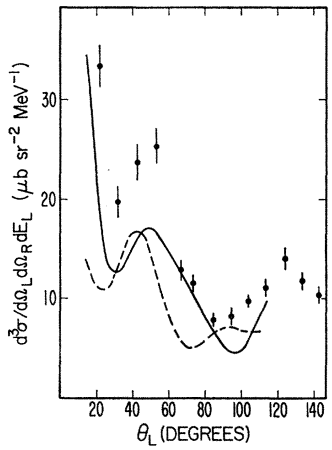

FIG. 10. The angular correlations computed with $R_F=1.33$ F (solid line) and 1.4 F (dashed line), using elastic-scattering potentials $V_F=58$ MeV, $W_F=7.5$ MeV, and $\langle r\rangle=2.79$ F.

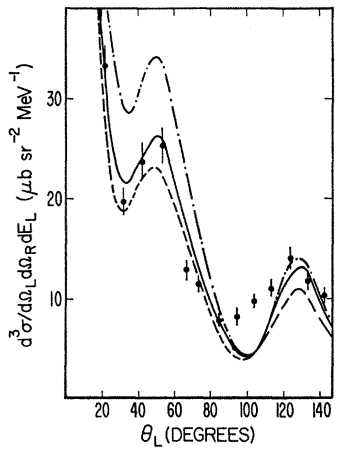

FIG. 11. Angular correlations computed with elastic-scattering optical-model potential magnitudes, $V_F=58$ MeV, $W_F=7.5$ MeV, and $R_F=1.33$ F. $\langle r\rangle=3.10$ F (full line), $\langle r\rangle=3.04$ F (dashed line), and $\langle r\rangle=3.23$ F (dotted line).

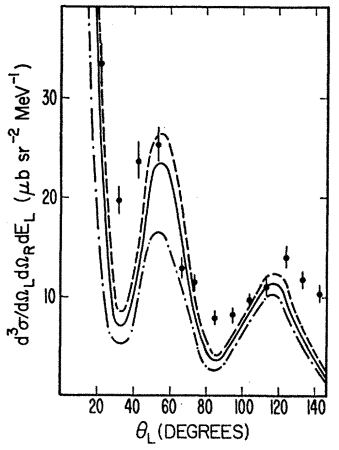

FIG. 12. The computed angular correlations using complete elastic scattering, optical-model potentials, and $\langle r\rangle=3.04$ F (dotted line) and 3.28 F (full line). The dashed line is the latter curve multiplied by a factor of 1.12.

eters. The only effective parameter left to vary is the bound-state radius R_B. The major discrepancy in the curve for set E (Fig. 6) was the low magnitude and the high ratio of the second to first peaks in the angular correlation. However, these were just the quantities which were most affected by increasing R_B. Figure 12 shows the curves calculated with set E and $\langle r\rangle=3.04$ (dotted line), and 3.28 F (full line). The dashed line is the last curve multiplied by 1.12.

V. CONCLUSIONS

The experimental measurements were made under conditions which allowed best comparison to distorted-wave calculations for the angular correlation. The angular and energy distributions confirm the distorted-wave direct interaction approach. In particular, the different angular correlation of events leaving B^{11} in different final states point out the necessity of measuring unique transitions. In spite of the high degree of data selectivity the experimental uncertainties were lower than had previously been obtained.

It is encouraging to note that the basic fixed-parameter theoretical calculations are not only well within an order of magnitude of the experimental results, but also give qualitative agreement for the angular distribution.

Very good theoretical fits to the data were obtained, provided that either the distortion effects or the nuclear size were overestimated. This could be done by increasing either the magnitude of the real part of the optical-model potential or the radial extent in an approximately VR^2 relationship. Shape changes were minimal as long as R_f was not increased beyond $1.33A^{1/3}$ F. A similar ambiguity occurred in the variation of R_B, the radius of the bound-state potential well, in place of the optical-model potential radius.

Increasing R_B, and thus $\langle r\rangle$, the rms radius of the bound-state wave function, was found to relatively raise the first maximum with respect to the second, with only small changes in the angular position. By increasing R_B beyond the previously used value, and using values taken from scattering experiments for the other parameters, a good shape fit can be obtained for realistic optical-model parameters with a magnitude only slightly below the experimental values. Since the energy threshold for S-state ejection prohibits the determination of the radius of the S state well at this low-incident energy, it is difficult to directly compare $\langle r\rangle$ with, for example, electron-scattering measurements.

The pseudopotential used to fit p-p scattering gave the best fit to the $(p,2p)$ experiment.

ACKNOWLEDGMENTS

The authors are very much indebted to Professor Ian McCarthy for the use of his computer code and for many helpful discussions. We also wish to express our thanks to S. Plunkett and the cyclotron staff for their valuable assistance.